Catalysis Communications 64 (2015) 86–90

Contents lists available at ScienceDirect

Catalysis Communications

journal homepage: www.elsevier.com/locate/catcom

Short communication

Characterization and catalytic performance of $\{Mo_2O_2S_2\}$-based oxothiomolybdenum cyclic clusters supported on mesoporous SBA-15

Zhifeng Xin *, Wei Wei, Min Chen, Ai-Quan Jia, Qian-Feng Zhang *

Institute of Molecular Engineering and Applied Chemistry, Anhui University of Technology, Ma'anshan, Anhui 243002, PR China

ARTICLE INFO

Article history:
Received 3 November 2014
Received in revised form 22 January 2015
Accepted 27 January 2015
Available online 29 January 2015

Keywords:
$Mo_2O_2S_2$-based wheels
Heterogeneous catalysis
Thiophene
Hydrodesulfurization

ABSTRACT

Cyclic polyoxothiomolybdate clusters containing $\{Mo_2O_2S_2\}$ building unit supported on SBA-15 have been prepared by immersion SBA-15 in the corresponding cluster's solution. The measurements of low angle X-ray diffraction (LXRD), nitrogen adsorption, transmission electron microscopy (TEM) and energy dispersive X-ray (EDX) spectroscopy indicated that the cyclic clusters were successfully loaded on SBA-15. The supported catalysts were tested in thiophene hydrodesulfurization at different temperatures, respectively. Results show that the supported catalysts have an excellent desulfurization catalytic performance for thiophene.

1. Introduction

Cyclic $[Mo_2O_2S_2]$-based molybdenum clusters result from the cyclic linking of $[Mo_2O_2S_2]^{2+}$ through double hydroxyl bridges around anionic templates, most commonly poly-carboxylate ligands [1,2]. This class of compounds exhibits unique electron structure and efficient electrocatalytic properties [3–5]. Molybdenum disulfide (MoS_2) and its derivatives have been widely used as catalysts for hydrodesulfurization (HDS) of petroleum [6,7]. The route preference depends on several factors such as support composition, promoter, S-containing molecules and catalyst preparation [7,8].

Cyclic $[Mo_2O_2S_2]$-based molybdenum clusters displayed flexible and adaptable cyclic oxothiomolybdenum rings exhibiting an open inner available cavity [9]. The encapsulated ligands should also have an influence upon the hydrodesulfurization (HDS) process. And these structural features afford this class of compounds more exciting catalytic properties. SBA-15 is highly ordered hexagonal mesoporous silica with high surface area [10]. As a catalyst, SBA-15 is not often directly used in reactions. So adding active elements onto the inner surface of the SBA-15 is a necessary process [11]. In this study, three $[Mo_2O_2S_2]$-based wheels: $K_{2-x}(NMe_4)_x$-$[I_2Mo_{10}O_{10}S_{10}(OH)_{10}(H_2O)_5]\cdot 20H_2O$ ($[(Mo_2O_2S_2)_n]$; $x = 1, 2$) and aromatic acid modified dodecamolybdenum: $Cs_2[Mo_{12}O_{12}S_{12}(OH)_{12}$-$(C_8H_4O_4)]\cdot 15H_2O\cdot 6DMF$ ($Mo_{12}BDC$), $K_3[Mo_{12}O_{12}S_{12}(OH)_{12}(C_9H_3O_6)]\cdot 22H_2O$ ($Mo_{12}BTC$) (DBC = 1,4-benzenedicarboxylate, BTC = 1,3,5-benzenetricarboxylate) [12] were loaded on an SBA-15 mesoporous material by the impregnation method. The thiophene hydrodesulfurization performance for the supported catalysts was investigated at four temperatures, respectively.

2. Experimental

2.1. Materials

Tetraethyl orthosilicate (98.0%), Pluronic P123 ($EO_{20}PO_{70}EO_{20}$) and thiophene were purchased from Energy Chemical, and used without further purification. SBA-15 was synthesized according to the reported method [11] and characterized with low angle X-ray diffraction (LAXRD) and N_2 adsorption measurement. All other chemicals were analytical grade and were purchased from Sinopharm Chemical Reagent Co., Ltd. (China).

2.2. Characterization

Powder X-ray diffraction (XRD) experiments were recorded on a Bruker D8 Advance (operating at 40 kV and 20 mA) with Ni-filtered Cu Ka radiation at 1.5406 (Å) with a speed of 0.1 min per step of 0.05°. The thermo-gravimetric analysis (TGA) was carried out on a Shimadzu DTG-60H thermo-gravimetric analyzer in the N_2 flow of 30 mL min^{-1} and the heating rate of 1 °C min^{-1}. TEM images were collected on a JEM-2100 electron microscope at 200 kV. N_2 adsorption/desorption isotherms were obtained at 77 K with a Micromeritics ASAP 2020 M + C system after the samples were first degassed at 120 °C for 6 h. ^1H NMR spectra were recorded at room temperature on a Bruker AC 400 MHz spectrometer using DMSO-d6 as the NMR solvents. IR spectra were taken from samples embedded in KBr pellets using a Nicolet 6700 FT-IR spectrophotometer. X-ray Photoelectron Spectroscopy

* Corresponding authors.
E-mail addresses: xinzf521@ahut.edu.cn (Z. Xin), zhangqf@ahut.edu.cn (Q.-F. Zhang).

http://dx.doi.org/10.1016/j.catcom.2015.01.025
1566-7367/

(XPS) was carried out on a Thermo ESCALAB 250XI multifunctional imaging electron spectrometer using the binding energy of C as the internal standard. The gas chromatography was obtained on a Shimadzu GC-2010 plus gas chromatograph connected a Rtx-wax column and a hydrogen flame ionization detector (FID) using N_2 as the carrier gas at a flow rate of 1.00 mL/min. Column temperature was first raised to 70 °C and maintaining for 4 min, and then raised to 120 °C with 10 °C/min and keeping for 6 min. The injection temperature and detector temperatures are 200 °C and 220 °C, respectively. Sample quantity is 0.5 μL with a split ratio of 10:1.

2.3. Preparation

2.3.1. $K_{2-x}(NMe_4)_x[I_2Mo_{10}O_{10}S_{10}(OH)_{10}(H_2O)_5]\cdot 20H_2O$ ($[(Mo_2O_2S_2)_n]$)

$K_{2-x}(NMe_4)_x[I_2Mo_{10}O_{10}S_{10}(OH)_{10}(H_2O)_5]\cdot 20H_2O$ ($[(Mo_2O_2S_2)_n]$) was synthesized according to reference [12]. IR (KBr pellet): the absorption peaks at 970, 525 and 488 cm^{-1} attributed to vibrations of ν(Mo═O), ν(Mo – OH – Mo) and ν(Mo – S – Mo), respectively. Pale orange crystals were obtained by dissolving 0.2 g of the yellow microcrystalline powder in 20 mL DMF/H_2O (1/5) and allowing the solution to stand for several days at room temperature.

2.3.2. $Cs_2[Mo_{12}O_{12}S_{12}(OH)_{12}(C_8H_4O_4)]\cdot 15H_2O\cdot 6DMF$ ($Mo_{12}BDC$)

$Cs_2[Mo_{12}O_{12}S_{12}(OH)_{12}(C_8H_4O_4)]\cdot 15H_2O\cdot 6DMF$ ($Mo_{12}BDC$) was synthesized according to reference [9]. 1H NMR (D6-DMSO/ppm): d = 11.43 (s, 4H), 10.56 (s, 8H), 5.07 ppm (s, 4H) (Fig. S2a); IR (KBr pellet): 970.51, ν = 1617(s), 1540(s), 1382(s), 966(s), 530(s) cm^{-1}. TGA: loses 15 lattice waters (ca. 9.4%) from room temperature to 47 °C, three lattice DMF molecules (ca. 7.4%) from 47 °C to 110 °C, six constitutive water molecules from the decomposition of 12 μ-OH (4%) and three coordinated DMF molecules (7.4%) between 110 and 389 °C, the loss after 389 °C corresponding to the ligand BDC (see Fig. S3b). The single crystal was obtained by dissolving the raw product in the mixed solvent of DMF/H_2O (1/1). The crystal structure was displayed in Fig. S1b.

2.3.3. $K_3[Mo_{12}O_{12}S_{12}(OH)_{12}(C_9H_3O_6)]\cdot 22H_2O$ ($Mo_{12}BTC$)

$K_3[Mo_{12}O_{12}S_{12}(OH)_{12}(C_9H_3O_6)]\cdot 22H_2O$ ($Mo_{12}BTC$) was synthesized according to reference [9]. ^1H NMR (DMSO-D_6): d = 10.04 (s, 12H), 5.93 ppm (s, 3H) (Fig. S2b); IR (KBr pellet): ν = 1610(s), 1544(s), 1438(s), 1370(s), 974(s), 927(s), 531 cm^{-1} (s). TGA: Loss of about 22 lattice water molecules below 270 °C and six constitutive water molecules (from the 12 OH bridging groups) from 270 to 430 °C (see Fig. S3c).

2.4. Synthesis of cluster anchored onto SBA-15: 150 mg SBA-15

Preparation of clusters anchored onto SBA-15: 150 mg SBA-15 was degassed at 120 °C under vacuum for 6 h. 20 mg $Mo_{12}S_{12}$, $Mo_{12}BDC$ or $Mo_{12}BTC$ was dissolved in deionized water which was degassed with N_2 bubbling for 15 min. The activated SBA-15 (1.5 g) was suspended into the above solution, and the mixture was stirred at 60 °C for 20 h. The excess water was removed using a rotary evaporator, and the resulting yellow solid was dried at 80 °C overnight. The product was washed with deionized water and MeOH until the filtrate became colorless. Finally the solid product was dried in an oven at 120 °C for 8 h and stored for further applications.

2.5. Catalyst testing

In a typical experiment, 0.1 g thiophene, 10 mL ethanol and 5 mg catalyst powder were added in Teflon-lined autoclave, and the reaction was performed under vigorous stirring at 200, 240, 280 and 320 °C for 20 h, respectively. The resulted mixture was filtered, and the filtrate was characterized with a gas chromatograph and gas chromatography mass spectrometry (GC–MS).

3. Results and discussion

3.1. Preparation and characterization of SBA-15 supported $[Mo_2O_2S_2]$-based wheels

$K_{2-x}(NMe_4)_x[I_2Mo_{10}O_{10}S_{10}(OH)_{10}(H_2O)_5]$ was prepared according to the literature [13]. The $[I_2Mo_{10}S_{10}O_{10}(OH)_{10}(H_2O)_5]^{2-}$ molecular consists of five $[Mo_2S_2O_2]$ units which connected to each other by hydroxo double bridges around two I^- anionic templates to form a ten membered ring [13]. In the cyclic structure of $Mo_{12}BDC$, each carboxylate group bridged the two adjacent Mo atoms of the same $[Mo_2S_2O_2]^{2+}$ moiety through single Mo – O interactions. Consequently, the four Mo atoms which connected to carboxylate groups retain an octahedral environment, whereas, the other eight Mo atoms display square-pyramidal arrangements (Fig. S1b) [9]. The structure of $Mo_{12}BTC$ can be described as a dodecanuclear ring encapsulated with a benzenetricarboxylate anion, each carboxylate group bridging two Mo centers (Fig. S1c) [9,12].

The ^1H NMR spectra of $Cs_2[Mo_{12}BDC]$ and $K_3[Mo_{12}BTC]$ were recorded in DMSO-d_6. The spectrum of $[Mo_{12}BDC]^{2-}$ (Fig. S2a) displayed three sharp resonances at δ = 5.06, 10.6 and 11.47 ppm with an integration of 1:2:1, respectively. The low frequency signal at δ = 5.07 ppm corresponded to the four aromatic protons of the encapsulated BDC guest, and the signals at 10.6 and 11.47 ppm corresponded to the twelve protons of twelve bridging hydroxyls. The ^1H NMR spectrum (Fig. S2b) of $K_3[Mo_{12}BTC]$ showed two sharp resonances at δ = 5.92 and 10.06 ppm with an integration of 1:4. The low frequency signal at δ = 5.07 ppm corresponded to the three aromatic protons of the encapsulated BTC guest, and the signals at 10.6 ppm corresponded to the twelve protons of twelve bridging hydroxyl [15].

The IR spectra of $[(Mo_2O_2S_2)_n]$/SBA-15 (Fig. S4a), $Mo_{12}S_{12}BDC$/SBA-15 (Fig. S5a) and $Mo_{12}S_{12}BTC$/SBA-15 (Fig. S6a) clearly showed bands associated with both the support and the molybdenum sulfide clusters. For instance, the strong peak for stretching of the Si – O – Si near 1085 cm^{-1}, bending vibration of Si – O – Si near 800 cm^{-1}, H – O – H bending vibrations of physisorbed water at 1634 cm^{-1}, and the vibrations near 1388, 1102, 1063, 969, 669 and 465 cm^{-1} can be referred as the characteristics of the $[Mo_2O_2S_2]$-based cyclic clusters [12–15]. The results further indicated that $[Mo_2O_2S_2]$-based cyclic clusters had been adsorbed in the support SBA-15.

The LXRD pattern of SBA-15, $[(Mo_2O_2S_2)_n]$/SBA-15, $Mo_{12}BDC$/SBA-15 and $Mo_{12}BTC$/SBA-15 showed a strong peak corresponding to (100) plane and two weak peaks corresponding to (110) and (200) planes of ordered hexagonal mesoporous materials (Fig. S7). The similarity in peak intensities and positions indicates that the structure of SBA-15 is unaffected by the activation process and the binding of molybdenum sulfide clusters. Nonetheless, the peaks corresponding to the (100) plane of $[(Mo_2O_2S_2)_n]$/SBA-15, $Mo_{12}BDC$/SBA-15 and $Mo_{12}BTC$/SBA-15 slightly shifted to lower angles and the peak intensity slightly decreased, which indicated a slight increase of the pore size and reduction of the period of ordered lattice. In the loading procedure, molybdenum sulfide clusters occupied the inner space of SBA-15 and filled part of the smaller pores, which lead to the pore size distribution shifted to larger direction and the peaks shifted to lower angles [6].

In good agreement with LXRD data, the transmission electron microscope (TEM) images (Fig. 1) of $[(Mo_2O_2S_2)_n]$/SBA-15, $Mo_{12}BDC$/SBA-15 and $Mo_{12}BTC$/SBA-15 displayed the similar ordered mesoporous structure with SBA-15. The particles or clusters loaded on the channel cannot be seen in the TEM images, but the EDX spectra (Fig. S8) showed the peaks of Mo and S, which indicated that the molybdenum sulfide clusters already loaded in the channels or on the surface. In the impregnation process, these clusters loaded on the channel surface didn't in the form of large nuclei but in the form of single molecular layer. The XRD spectra (Fig. S9) showed the amorphous structure of $[(Mo_2O_2S_2)_n]$/SBA-15, $Mo_{12}BDC$/SBA-15 and $Mo_{12}BTC$/SBA-15, which also indicated

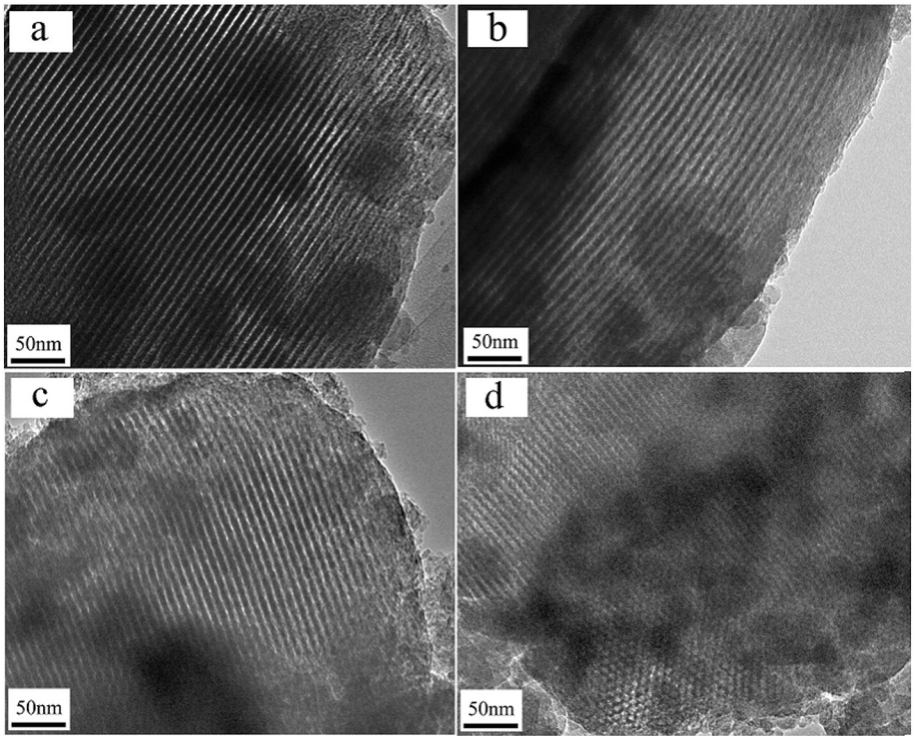

Fig. 1. TEM images of SBA-15 (a), $[(Mo_2O_2S_2)_n]$/SBA-15 (b), Mo_{12}BDC/SBA-15 (c), and Mo_{12}BTC/SBA-15 (d).

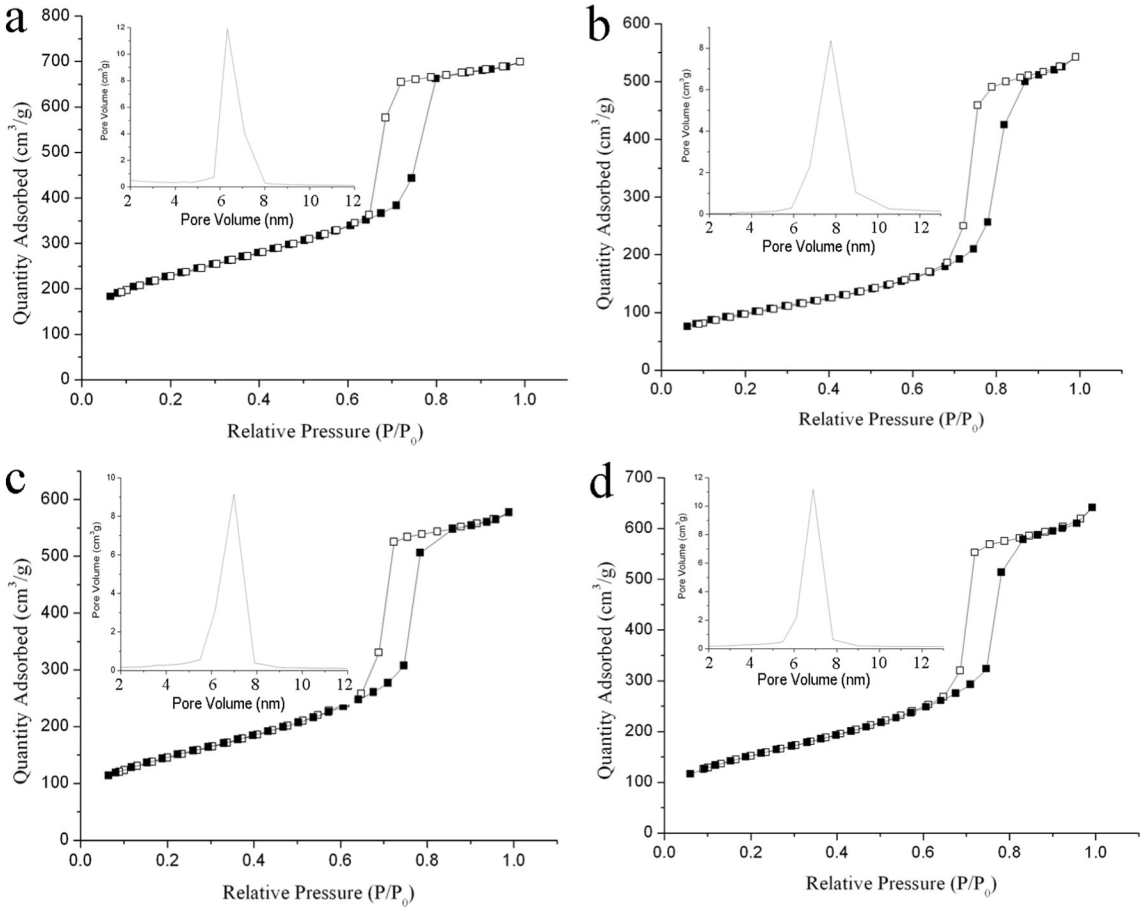

Fig. 2. N_2 sorption isotherms of SBA-15 (a), $[(Mo_2O_2S_2)_n]$/SBA-15 (b), Mo_{12}BDC/SBA-15 (c), and Mo_{12}BTC/SBA-15 (d). The insets were the corresponding pore size distribution curves.

that the cluster $(Mo_2O_2S_2)_n$, $Mo_{12}BDC$ or $Mo_{12}BTC$ uniformly dispersed on the pore wall of SBA-15.

The pore structure of the sample of SBA-15, $[(Mo_2O_2S_2)_n]$/SBA-15, $Mo_{12}S_{12}BDC$/SBA-15 and $Mo_{12}BTC$/SBA-15 was also detected by low pressure N_2 sorption measurement at 77 K. The characteristic shape of N_2 sorption isotherms (type IV isotherm with an H1 hysteresis loop) of SBA-15 did not change by the loading of the molybdenum sulfide clusters, which indicated that the original pore structure of SBA-15 is maintained after the impregnation step. The obvious decrease of N_2 uptakes indicated that the polyoxothiomolybdate clusters occupied the partial inner surface of SBA-15 through the impregnation procedure (Fig. 2) [6]. The pore width distributions of SBA-15, $[(Mo_2O_2S_2)_n]$/SBA-15, $Mo_{12}S_{12}BDC$/SBA-15 and $Mo_{12}BTC$/SBA-15 were all from 5.6 nm to 10 nm, but the average pore width of $[(Mo_2O_2S_2)_n]$/SBA-15 (7.15 nm), $Mo_{12}S_{12}BDC$/SBA-15 (6.91 nm) and $Mo_{12}BTC$/SBA-15 (7.34 nm) was slightly larger than that of bare SBA-15 (6.32 nm), which is agreement with that of LAXRD. From the N_2 sorption isotherms and pore distribution curves (Fig. 2 inset), it is evident that the loading of the clusters into the SBA-15 slightly decreased its surface area and pore volume. Due to part surface area and the micro-pore volume was occupied by clusters, the proportion of macro-pore increased and average pore diameter slightly increased. The data of the BET surface area, pore volume and average pore diameter of the samples are presented in Table 1.

3.2. Stability of the supported catalysts

The shape of TGA curves (Fig. S10) of the supported catalysts is similar to that of pure clusters (Fig. S4). For $[(Mo_2O_2S_2)_n]$/SBA-15, the weight loss before 150 °C attributed to the adsorbed water, lattice water and coordinated water, and between 150 and 350 °C attributed to the constitutive water molecules (from the OH bridging groups). As for $Mo_{12}S_{12}BDC$/SBA-15, the weight loss before 398 °C attributed to the adsorbed solvent, lattice water molecules, coordinated water and six constitutive water molecules (from the sixteen OH bridging groups). And for $Mo_{12}BTC$/SBA-15, loss of about adsorbed water and lattice water between room temperature and 270 °C, six constitutive water molecules (from the 12 OH bridging groups) between 270 and 430 °C [9]. So the lattice water, coordinated water and constitutive water molecules of the clusters may be lost in the catalytic procedure from 200 °C to 320 °C, however, the IR spectra (Figs. S4–S5) indicated that the Mo – S – Mo bond (the vibration at 493 cm^{-1}) of the three supported catalysts still exists after being catalyzed from 200 °C to 320 °C. The Mo (3*d*) XPS (Fig. S11) curves of $[(Mo_2O_2S_2)_n]$/SBA-15 indicated that the Mo^{4+} (228.6 eV, Fig. S11d, e) appeared after catalyzed at 280 °C and 320 °C.

3.3. Temperature-programed reduction (TPR) experiment

33.0 mg of sample was added into a quartz U-tube reactor connected to a thermal conduction detector. In order to remove the water from the catalysts, the samples were pretreated in flowing dry N_2 (30 mL/min) at 100 °C for 2 h. After cooled to room temperature, the gas mixture of hydrogen/argon (9%/91%) passed through the U-tube reactor at a flow rate of 20 mL/min. And the temperature of the reactor was increased to 700 °C at a heating rate of 10 °C/min. The hydrogen absorption appeared from 280 °C to 340 °C and reached a peak at 320 °C (Fig. S12), which corresponded to the reduction of molybdenum (Mo^{5+} to Mo^{4+}). This result was in accordance with that of XPS.

Table 1
Textural properties of the supported catalysts.

Samples	BET surface area (m^2/g)	Pore volume (cm^3/g)	Pore width (nm)
$[(Mo_2O_2S_2)_n]$/SBA-15	498.45	0.89	7.15
$Mo_{12}S_{12}BDC$/SBA-15	516.86	0.89	6.91
$Mo_{12}S_{12}BTC$/SBA-15	540.01	0.99	7.34
SBA-15	792.23	1.08	6.32

3.4. Effect of the temperature on the catalytic performance

Catalytic activity of the catalysts was evaluated in a stainless autoclave reactor in a temperature range of 200–320 °C for 20 h. The thiophene/ethanol system after hydrodesulfurization catalyzed by these supported catalysts at different temperatures was characterized by gas chromatography (Figs. S13–S15). Fig. 3 displayed the conversion rate and selectivity of thiophene desulfurization catalyzed by the supported catalysts. The results of GC–MS testing indicated the desulfurization

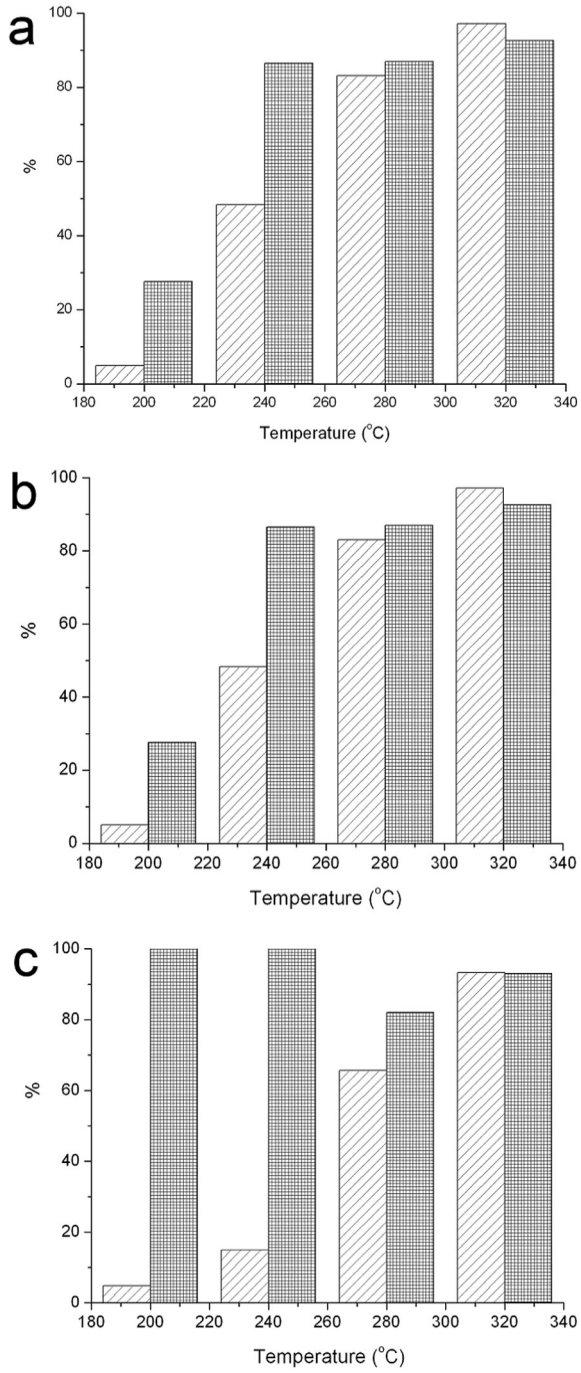

Fig. 3. Conversion rate (▨) and selectivity (▦) of thiophene hydrodesulfurization for the catalysts of $[(Mo_2O_2S_2)_n]$/SBA-15 (a), $Mo_{12}BDC$/SBA-15 (b), and $Mo_{12}BTC$/SBA-15 (c), respectively, at 200 °C, 240 °C, 280 °C, and 300 °C.

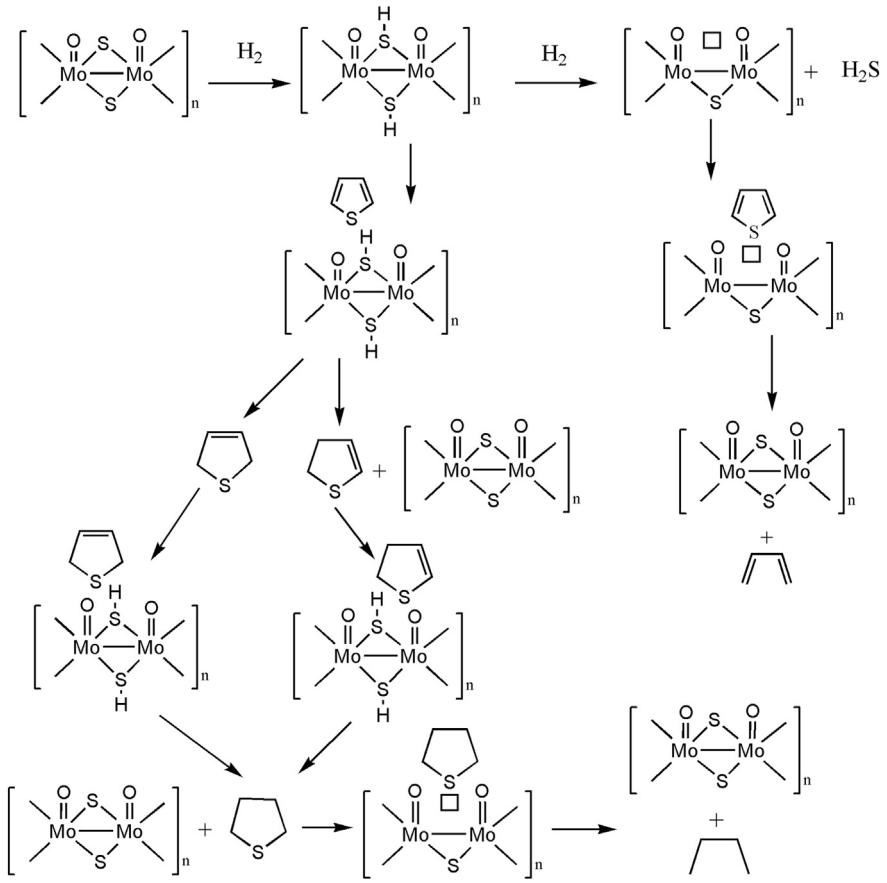

Fig. 4. Possible mechanism of thiophene hydrodesulfurization on cyclic $[Mo_2O_2S_2]$-based catalyst.

products of 1-butanol and tetrahydro-thiophene. The selectivity was calculated by the ratio of the yield of 1-butanol to the conversion rate of thiophene. Fig. 3 indicated that the catalytic activity of the supported catalyst increased with increasing temperature. After 280 °C, the thiophene conversion rate increased obviously, which is in accordance with the result of H_2-TPR experiment, and HDS selectivity ratio is above 90%.

In HDS catalytic reactions, the H_2 molecule was adsorbed on the catalyst in the form of S–H bond which can migrate to the adsorbed thiophene [16]. The desulfurization mechanism of thiophene included two procedures (Fig. 4): hydrodesulfuzation and direct desulfurization. The hydrogen atom transferred from S–H bond to the C═C of thiophene, which can saturate the aromatic thiophene ring making the desulfurization easier, and then break the C – S bond. In the desulfurization step, the hydroxyl in the reaction system attacked and connected with the butyl to form 1-butanol.

4. Conclusions

The three clusters $[(Mo_2O_2S_2)_n]$, Mo_{12}BDC and Mo_{12}BTC were supported on SBA-15 with the impregnation method and were characterized by LXRD, TEM, IR spectra, EDX and N_2 sorption measurements. The desulfurization catalytic activities of the supported catalysts were investigated with thiophene at 200, 240, 280 and 320 °C, respectively. The results indicated that these $[Mo_2O_2S_2]$-based cyclic clusters exhibit an excellent desulfurization catalytic activity at relatively lower temperature, which is obviously higher than those of $(Co)MoS_2$ catalysts [17].

Acknowledgments

This work was financially supported by the National Natural Science Foundation of China (grant nos. 21101003 and 90982008).

Appendix A. Supplementary data

Supplementary data to this article can be found online at http://dx.doi.org/10.1016/j.catcom.2015.01.025.

References

[1] E. Cadot, F. Sécheresse, Chem. Commun. (2002) 2189–2197.
[2] J.F. Lemonnier, S. Duval, S. Floquet, E. Cadot, Isr. J. Chem. 51 (2011) 290–302.
[3] A. Hijazi, J.C. Kemmegne-Mbouguen, S. Floquet, J. Marrot, C.R. Mayer, V. Artero, E. Cadot, Inorg. Chem. 50 (2011) 9031–9038.
[4] S. Duval, S. Floquet, C. Simonnet-Jégat, J. Marrot, R.N. Biboum, B. Keita, L. Nadjo, M. Haouas, F. Taulelle, E. Cadot, J. Am. Chem. Soc. 132 (2010) 2069–2077.
[5] B. Keita, S. Floquet, J.F. Lemonnier, E. Cadot, A. Kachmar, M. Bénard, M.M. Rohmer, L. Nadjo, J. Phys. Chem. C 112 (2008) 1109–1114.
[6] D. Valencia, T. Klimova, Appl. Catal. B 129 (2013) 137–145.
[7] A. Cho, J.J. Lee, J.H. Koh, A. Wang, S.H. Moon, Green Chem. 9 (2007) 620–625.
[8] (a) D. Valencia, T. Klimova, Catal. Today 166 (2011) 91–101;
(b) A. Tuxen, J. Kibsgaard, H. Gøbel, E. Lægsgaard, H. Topsøe, J.V. Lauritsen, F. Besenbacher, ACS Nano 4 (2010) 4677–4682;
(c) J. Kibsgaard, A. Tuxen, K.G. Knudsen, M. Brorson, H. Topsøe, E. Lægsgaard, J.V. Lauritsen, F. Besenbacher, J. Catal. 272 (2010) 195–203.
[9] J.F. Lemonnier, S. Floquet, J. Marrot, E. Terazzi, C. Piguet, P. Lesot, A. Pinto, E. Cadot, Chem. Eur. J. 13 (2007) 3548–3557.
[10] (a) D. Zhao, J. Feng, Q. Huo, N. Melosh, G.H. Fredrickson, B. Chmelka, G.D. Stucky, Science 279 (1998) 548–552;
(b) B. Li, W. Ma, J. Liu, C. Han, S. Zuo, X. Li, Catal. Commun. 13 (2011) 101–105.
[11] A. Taguchi, F. Schuth, Microporous Mesoporous Mater. 77 (2005) 1–45.
[12] E. Cadot, B. Salignac, S. Halut, F. Sécheresse, Angew. Chem. Int. Ed. 37 (1998) 611–613.
[13] E. Cadot, B. Salignac, J. Marrot, A. Dolbecq, F. Sécheresse, Chem. Commun. (2000) 261–262.
[14] G.R. Bardajee, R. Malakooti, I. Abtin, H. Atashin, Microporous Mesoporous Mater. 169 (2013) 67–74.
[15] A. Hijazi, J.C. Kemmegne-Mbouguen, S. Floquet, et al., Dalton Trans. 42 (2013) 4848–4858.
[16] X.-Q. Yao, Y.-W. Lia, H. Jiao, J. Mol. Struct. THEOCHEM 726 (2005) 81–92.
[17] M. Li, H. Li, F. Jiang, Y. Chu, H. Nie, Catal. Today 149 (2010) 35–39.